



HAL
open science

Kinematics and dynamics of pedestrian head ground contact: A cadaver study

Shi Shang, Catherine Masson, David Teeling, Max Py, Quentin Ferrand,
Pierre-Jean Arnoux, Ciaran Simms

► **To cite this version:**

Shi Shang, Catherine Masson, David Teeling, Max Py, Quentin Ferrand, et al.. Kinematics and dynamics of pedestrian head ground contact: A cadaver study. *Safety Science*, 2020, 127, pp.104684. 10.1016/j.ssci.2020.104684 . hal-03228376

HAL Id: hal-03228376

<https://amu.hal.science/hal-03228376v1>

Submitted on 18 May 2021

HAL is a multi-disciplinary open access archive for the deposit and dissemination of scientific research documents, whether they are published or not. The documents may come from teaching and research institutions in France or abroad, or from public or private research centers.

L'archive ouverte pluridisciplinaire **HAL**, est destinée au dépôt et à la diffusion de documents scientifiques de niveau recherche, publiés ou non, émanant des établissements d'enseignement et de recherche français ou étrangers, des laboratoires publics ou privés.



Distributed under a Creative Commons Attribution - NonCommercial - NoDerivatives 4.0 International License

Kinematics and dynamics of pedestrian head ground contact: a cadaver study

Shi Shang¹, Catherine Masson², David Teeling¹, Max Py², Quentin Ferrand², Pierre-Jean Arnoux²,
Ciaran Simms^{1*}

¹ Trinity Centre for Bioengineering, Trinity College Dublin, Ireland

² Laboratoire de Biomécanique Appliquée (IFSTTAR – Université de la Méditerranée), France

*Corresponding Author (Email: csimms@tcd.ie)

Abstract

Pedestrians struck by vehicles are generally injured by the primary vehicle contact but also the secondary ground contact. However, experimental evidence for ground contact injuries is limited. Here we report on six staged cadaver tests at 20-30km/h with passenger cars/vans in which we recorded the whole process from first pedestrian contact until after the end of the ground contact is complete using high-speed video and accelerometers mounted in the cadavers. Results show distinct phases for pedestrian flight and ground contact in addition to the already established vehicle contact phases. No skull fractures were observed in any of the tests. However, for the speed range tested, the linear and angular head injury risk (evaluated using HIC/3ms & BrIC respectively) is generally higher from the ground contact compared to the vehicle contact. Although not yet clearly understood, angular head injury risk during ground contact is higher for the 20km/h tests compared to the 30km/h tests. A good comparison was observed with respect to previously predicted ground contact mechanisms and head impact speeds from multibody modelling. These results emphasize the importance of ground related injuries to pedestrians when struck by vehicles at speeds of 20-30km/h and provide a unique dataset for computational model validation of pedestrian ground contact.

Keywords

Pedestrians, vehicle contact, ground contact, cadaver test analysis

1. Introduction

The World Health Organization reports nearly 300,000 pedestrian fatalities annually (WHO, 2013), with many more injured. Injuries occur during the primary vehicle contact and, following separation from the vehicle, significant additional injuries often occur during ground contact. In early collision reconstruction work, Ashton and Mackay (Ashton and Mackay, 1983) showed that for vehicle impact speeds below about 25km/h, ground contact injuries exceed those of vehicle contact, but at higher speeds injuries from vehicle contacts predominate.

Pedestrian injuries in contacts with vehicles are generally well understood, with vehicle speed/shape/stiffness and pedestrian age/height/stance all influencing injury outcome (Kalra et al., 2016; Li et al., 2017a; Li et al., 2017b; Niebuhr et al., 2016; Rosen et al., 2011; Shang et al., 2018b; Simms, 2005; Simms and Wood, 2009). However, pedestrian ground contact involves a wide range of contact orientations and a complex combination of slide, roll and bounce to rest. The resultant injury mechanisms are not well understood as significant challenges persist in predicting the kinematics of this long timeframe event and in attributing injuries observed to either vehicle or ground contact (Simms and Wood, 2009). However, recent analysis of the German collision database GIDAS showed that the head, thorax and spine dominate AIS4-5 ground contact injuries,

43 and ground contact injury severity increases with pedestrian age and vehicle speed (Shang et al.,
44 2018b). For collisions below 40 km/h, about two thirds of pedestrian injury costs were attributed to
45 ground contact, emphasising the importance of ground contact injuries for low impact speeds
46 (Shang et al., 2018b). Badeo-Romero and Lenard assessed UK collisions and also found a
47 significant role for ground contact (Badea-Romero and Lenard, 2013).

48 Of particular interest is the manner in which pedestrian ground contact injuries are influenced
49 by vehicle speed and design in the speed range 20-40 km/h, since this could lead to vehicle-based
50 methods to reduce the severity of ground contact injuries in cases where pedestrian injuries from
51 vehicle contact are mostly survivable. Computational modelling studies have posited various
52 relationships between vehicle shape and ground contact injuries (Crocetta et al., 2015; Gupta et al.,
53 2015; Gupta and Yang, 2013; Kendall et al., 2006; Tamura and Duma, 2011; Tamura et al., 2014; Xu
54 et al., 2016). In particular, Crocetta et al. (Crocetta et al., 2015) reported on six identifiable ground
55 contact “mechanisms” distinguished by the amount of whole body rotation of the pedestrian prior to
56 ground contact, with average head impact speed varying between the different mechanisms. Some
57 support for identifying an influence of vehicle design on pedestrian ground contact was found by
58 Shang et al (Shang et al., 2018b) who used collision data to show that the normalised bonnet
59 leading-edge height (bonnet height/hip height) is a risk factor for adult pedestrian AIS2+ ground-
60 related head injuries. Further, Han et al. (Han et al., 2018) found from video analysis of real-world
61 collisions that vehicle front shape and impact speed both influence ground contact kinematics.
62 However, no pedestrian models are validated for ground contact and establishing initial conditions
63 and injury outcomes in real world video cases is challenging.

64 Cadaver tests provide model validation data and have the potential to greatly strengthen our
65 understanding of pedestrian ground contact. However, previous tests have mainly focused on
66 vehicle contact, with limited reference to ground contact (Kerrigan et al., 2007; Masson et al., 2007;
67 Paas et al., 2015; Subit et al., 2008) or else crash test dummies were used (Hamacher et al., 2011;
68 Taneda et al., 1973). In early work, (Cavallero et al., 1983) concluded that head-ground contact
69 location and speed could not be predicted from vehicle shape. However, tests were performed only
70 at 32 km/h, vehicle shapes have changed substantially and no ground contact kinematics or injuries
71 were reported. More recently, cadaver studies performed in the US and France have used a range
72 of vehicle shapes and pedestrian sizes (Kerrigan et al., 2007; Paas et al., 2015; Subit et al., 2008),
73 but ground contact kinematics/injuries were not evaluated. In fact, the sequence of pedestrian
74 motion following head contact on vehicle has received little attention and is poorly described.

75 In summary, pedestrian ground contact kinematics remain poorly understood. Model predictions
76 of ground contact mechanisms have been presented, but validation is lacking. Real-world collisions
77 show the importance of ground contact, but the role of vehicle design in mediating pedestrian
78 ground contact injury remains uncertain and existing cadaver data is limited. Accordingly, the aims
79 of the current study are to:

- 80 1) perform staged vehicle impact tests using cadavers to study the kinematic chain of
81 events in a pedestrian collision, starting with first vehicle contact and ending after the
82 pedestrian strikes the ground.
- 83 2) assess pedestrian post-impact kinematics as well as head ground contact, including
84 linear and rotational components of head injury risk.
- 85 3) assess potential interactive effects of vehicle speed and normalised bonnet leading edge
86 height on pedestrian head injury risk during ground contact.

87 **2.Methods**

88 **2.1 Cadaver Test Setup**

89 As part of the Faculty of Medicine of Marseille, the Laboratory of Applied Biomechanics is
 90 enabled to perform full body human testing from body donations. Six cadaver tests were conducted
 91 to study pedestrian ground contact at Aix-Marseille Université: Faculté de Médecine-secteur Nord
 92 Marseille, see Table 1. Winckler’s preparation (Winckler, 1974) or zinc chloride (Goodarzi et al.,
 93 2017) was used for tissue preservation. For each subject, up to 54 anthropometric measures were
 94 performed, and the external anthropometries are listed in Appendix A. The study was approved by
 95 the Ethical Committee of Aix-Marseille University. Three vehicle types (Appendix B) were tested to
 96 achieve different normalized bonnet leading edge heights (NBLEH), and each vehicle type was
 97 tested twice under similar conditions (different cadavers but approximately the same initial stance).
 98 Damaged vehicle components were replaced as necessary. The expected ground contact
 99 “mechanism” (Appendix C) based on the simulation study by Crocetta et al (Crocetta et al., 2015)
 100 for each case is also shown. Five 1000 fps cameras captured the whole pedestrian trajectory
 101 (Appendix D). Impact speeds of 20 or 30km/h were applied.
 102

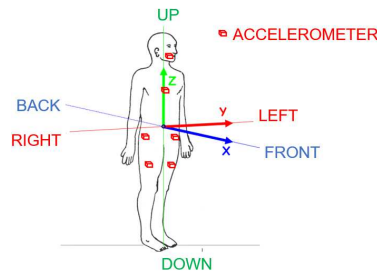
Table 1: Summary of tests performed

Test number	Vehicle speed (km/h)	Pedestrian/ vehicle size	NBLEH	Expected mechanism (M1-M6) (Crocetta et al., 2015) – see Appendix C
Test 01	30.5	Peugeot 307 (sedan) + (Male, 88 y/o, 1.74m, 66kg)	0.7	M1 (most frequent) or M3 (less frequent) mechanism for adults struck by compact car at 30 kph – Figure 8 in (Crocetta et al., 2015)
Test 02	30.4	Peugeot 307 (sedan) + (Male, 83 y/o, 1.72m, 69kg)	0.7	
Test 03	20.4	Citroen C4 (compact)+ (Male, 94 y/o, 1.67m, 64kg)	0.9	M2 (most frequent mechanism for adults struck by any vehicle at 20 kph) - Figure 7 in (Crocetta et al., 2015)
Test 04	21.0	Citroen C4 (compact)+ (Male, 83 y/o, 1.67m, 55kg)	0.9	
Test 05	30.1	Renault Kangoo II (van)+ (Female, 94 y/o, 1.58m, 38kg)	1.2	M2 (most frequent) or M1 (less frequent) mechanism for adults struck by a Van at 30 kph - Figure 8 in (Crocetta et al., 2015)
Test 06	30.4	Renault Kangoo II (van)+ (Male, 86 y/o, 1.62m, 69kg)	1.1	

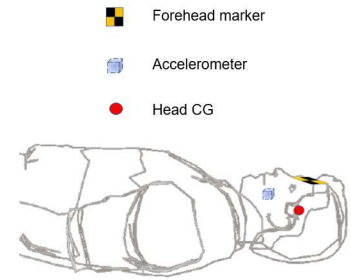
103
 104 The cadavers were held by a magnetic locking system which automatically released just
 105 before vehicle contact, see Figure 1a. Fiducial markers recorded landmark positions on the head,
 106 extremities, pelvis and chest. The approximate initial lower extremity joint angles are shown in
 107 Appendix E. Full braking ($\mu \approx 0.8$) was applied after first pedestrian contact. Six triaxial
 108 accelerometers (10 kHz sample rate, -3dB AA hardware filter) were inserted in the cadavers (see
 109 Figure 1b): one was inserted in the chest, two were screwed on the left and right thigh bones, two
 110 were inserted in the ilium (left and right side) and one was inserted in the mouth to represent an
 111 approximate head CG. The mouth accelerometer was pressed against the palate and expanding
 112 foam was used to fill the mouth cavity. The accelerometer position was maintained during setting
 113 and curing. When dry, the surplus was removed and the head was equipped with a hood. Only the
 114 head accelerometer data is presented in this paper.



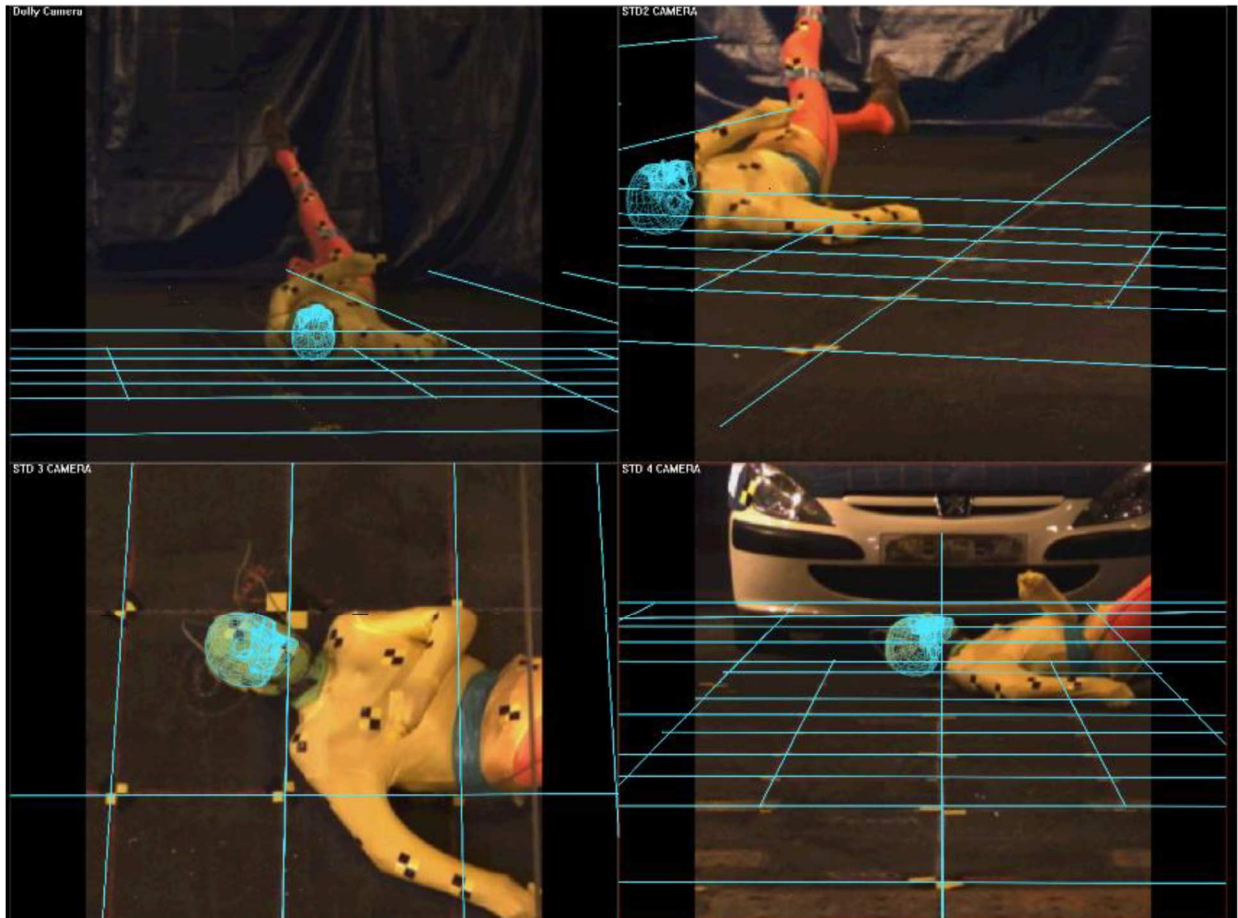
(a)



(b)



(c)



(d)

Figure 1: (a) Pre-impact scenario; (b) accelerometer positions and nominal orientations; (c) head accelerometer, CG and forehead marker positions; (d) Sample head MBIM matching using multi-view camera images

115 **2.2 Video Data Analysis**

116 Head trajectories in the X (vehicle forward direction) and Z (vertically upward) directions were
 117 estimated by manually tracking the location of the forehead marker (Figure 1c) every 10ms (or every
 118 1ms during head contacts). Linear velocities were obtained using a central difference scheme.
 119 Rotational kinematics for the head during both vehicle and ground contacts were estimated using
 120 Model Based Image Matching (MBIM), introduced by (Bahr and Krosshaug, 2005) and recently
 121 applied to head impacts (Tierney et al., 2015; Tierney et al., 2018). MBIM uses multiple camera

122 views to build an environment based on known background dimensions. The user manually fitted a
 123 skull model (from the Poser platform) to the envelope of the head from videos at each time frame
 124 (1ms), see Figure 1(d). The rotation matrix for the head was then extracted at each time step, and a
 125 central difference scheme was used to compute body local angular velocity components. Each case
 126 was reconstructed by two independent researchers. Tierney et al (Tierney et al., 2018) previously
 127 reported that MBIM is repeatable for both single and multiple researchers.
 128

129 2.3 Head injury assessments

130 The Head Injury Criterion (*HIC*) is commonly used to assess skull fracture risk (Hutchinson et
 131 al., 1998; Versace, 1971):
 132

$$133 \quad HIC = \left\{ \left[\frac{1}{t_2 - t_1} \int_{t_1}^{t_2} a_m(t) dt \right]^{2.5} (t_2 - t_1) \right\}_{max},$$

134 where t_1 and t_2 are initial/final times (in seconds) to maximize *HIC*, and a_m is the resultant head
 135 CG acceleration (units of g), with time duration ($t_2 - t_1$) constrained to be less than 15 ms. However,
 136 since our accelerometers were fixed in the mouth instead of the head CG (Figure 1c) for practical
 137 reasons, strict computation of *HIC* was not possible with our available instrumentation. Instead, we
 138 define the “approximate Head Injury Criterion” (*aHIC*), calculated by applying the *HIC* computation
 139 to our head accelerometer data. To verify this approach, a virtual sensor was inserted in the same
 140 location in the 50th percentile male MADYMO pedestrian model to check the difference between *HIC*
 141 and *aHIC* in a simulation similar to those in (Shang et al., 2018a). Results showed an approximate
 142 10% difference, suggesting this approach is reasonable. The reported threshold for *HIC* is 700 for
 143 an approximate 30% chance of skull fracture (Schmitt et al., 2010). The 3ms acceleration criterion
 144 for the head was also calculated, used in regulations (ECE, 2008, 2010) to assess energy
 145 dissipation in a vehicle, and it requires that accelerations of duration greater than 3ms do not
 146 exceed 80g (Got et al., 1978).

147 To assess the risk of rotationally induced brain injuries, the Brain Injury Criterion (*BrIC*)
 148 (Takhounts et al., 2013) during vehicle and ground contact was assessed using the MBIM results.
 149 The *BrIC* is associated with traumatic brain injuries (TBI), which has been used to assess the brain
 150 injuries of vulnerable road users (Gabler et al., 2016; Gabler et al., 2018; Kimpara and Iwamoto,
 151 2012; Mueller et al., 2015) and athletes (Aomura et al., 2016). (Gabler et al., 2018) also proposed
 152 another criterion, UBrIC, to assess rotationally induced brain injury. However, evaluation of UBrIC
 153 requires a measure of angular acceleration which could not be reliably predicted with the available
 154 equipment. The *BrIC* score is found from the peak body local head angular velocities:

$$155 \quad BrIC = \sqrt{\left(\frac{\omega_x}{\omega_{xC}} \right)^2 + \left(\frac{\omega_y}{\omega_{yC}} \right)^2 + \left(\frac{\omega_z}{\omega_{zC}} \right)^2},$$

156 where ω_x , ω_y and ω_z are the peak head angular velocity components and $\omega_{xC} = 66.3rad/s$,
 157 $\omega_{yC} = 56.5rad/s$, $\omega_{zC} = 42.9rad/s$ are critical values proposed by Takhounts et al (Takhounts et
 158 al., 2013). The *BrIC* score was used to estimate the risk of an AIS3+ brain injury (Takhounts et al.,
 159 2013) in this study.
 160

161 **3.Results**

162 **3.1 Pedestrian kinematics during the whole process of vehicle impact**

163 Figure 2 and Table 2 summarize overall kinematics, impact timings and intervals of the impact
 164 phases, with timings determined from the head accelerometer. Establishing the approximate contact
 165 time interval for both head-to-vehicle and head-to-ground contact in all tests was achieved by a
 166 combination of the filtered accelerometer and video data. For the onset of contact a sharp change in
 167 the accelerometer time curve could be readily identified in each case and verified by comparison
 168 with the video data. Establishing the effective end time for each contact was more challenging and
 169 no general criterion could be applied. Instead the end time was estimated by inspecting the
 170 acceleration time-history and comparing this to the video data. The time of first contact between the
 171 vehicle and pedestrian is t_0 . The pedestrian rotates onto the bonnet during phase 1. The time of first
 172 head impact on vehicle is t_1 . The pedestrian moves with the vehicle in phase 2. At t_2 , the pedestrian
 173 separates from the vehicle due to braking. The pedestrian has a flight period (phase 3) until t_3 , when
 174 first ground contact occurs (any body part). Then t_4 is the time of first head ground contact (in some
 175 cases $t_4 = t_3$). There follows a period of slide/roll and bounce (phase 4) until the pedestrian becomes
 176 stationary at t_5 . Appendix F shows the pedestrian head trajectories in the X (horizontal) and Z
 177 (vertical) directions for all six tests. Head impact locations on the vehicle are shown in Appendix G.
 178

Table 2: Key vehicle and ground contact events (s)

Key time	t_0	Phase 1 duration	t_1	Phase 2 duration	t_2	Phase 3 duration	t_3	t_4	Phase 4 duration	t_5
Description	1 st vehicle pedestrian contact		1 st head vehicle contact		pedestrian & vehicle separate		1 st ground contact (any)	1 st head ground contact		Pedestrian at rest
Test 01 (30.5 kph)	0	0.145	0.145	0.625	0.770	0.203	0.973	0.995	1.270	2.265
Test 02 (30.4 kph)	0	0.153	0.153	0.557	0.710	0.276	0.986	0.986	1.019	2.005
Test 03 (20.4 kph)	0	-	none	-	0.834	0.195	1.029	1.180	1.303	2.483
Test 04 (21 kph)	0	0.169	0.169	0.571	0.740	0.185	0.905	0.970	1.824	2.794
Test 05 (30.1 kph)	0	0.098	0.098	0.549	0.647	0.213	0.86	0.860	1.374	2.234
Test 06 (30.4 kph)	0	0.110	0.110	0.617	0.727	0.202	0.929	0.936	1.193	2.129

179

180

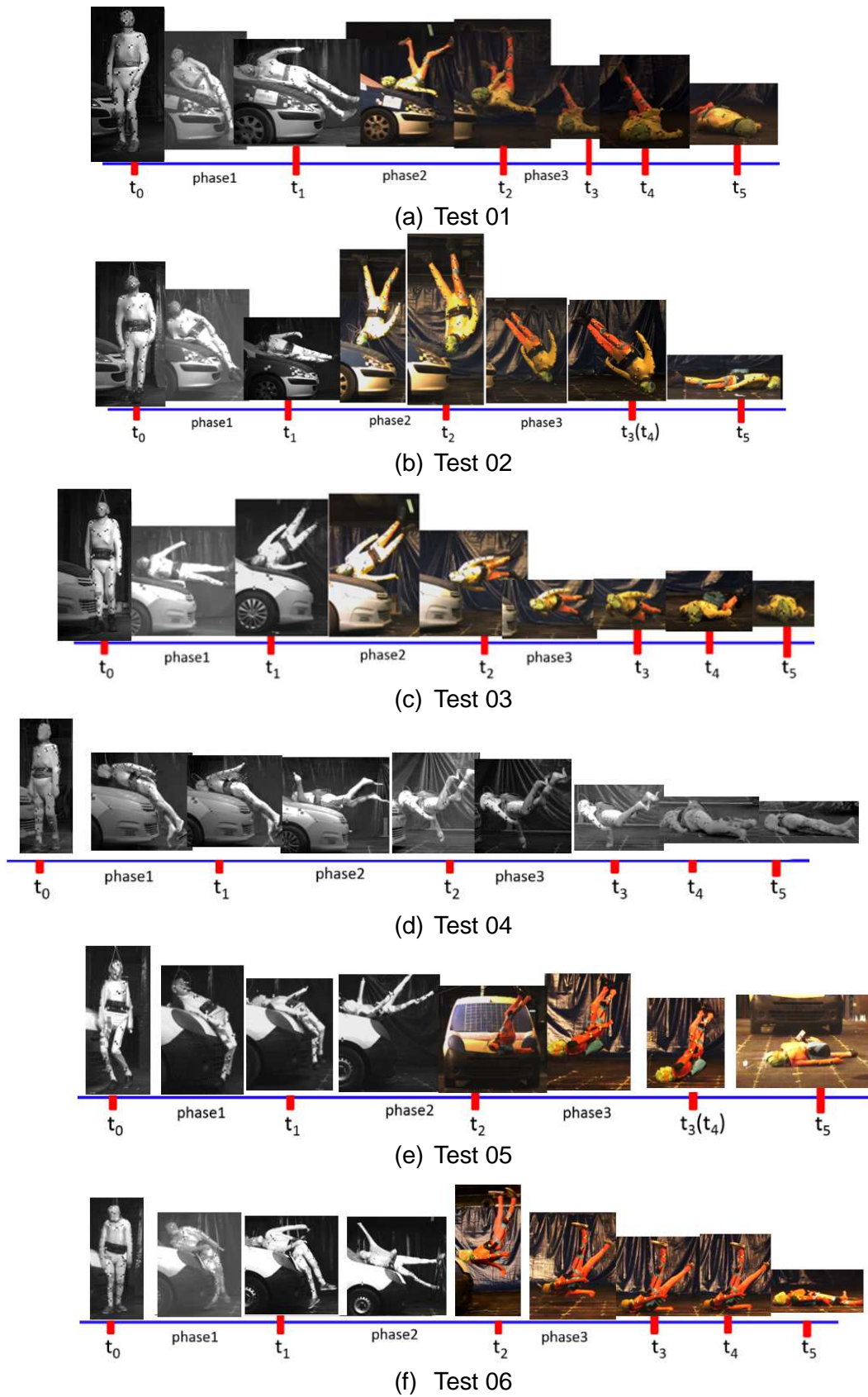
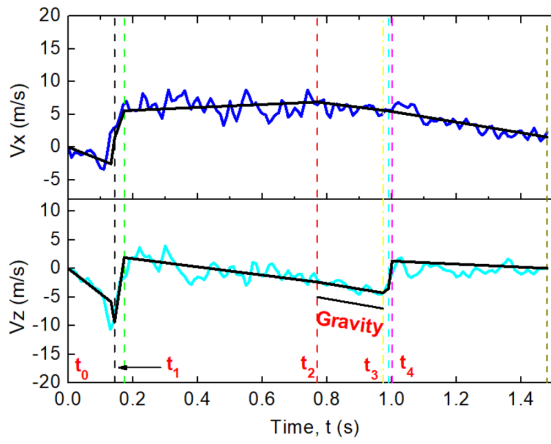


Figure 2: Sequences of vehicle-pedestrian impact for the six cadaver tests

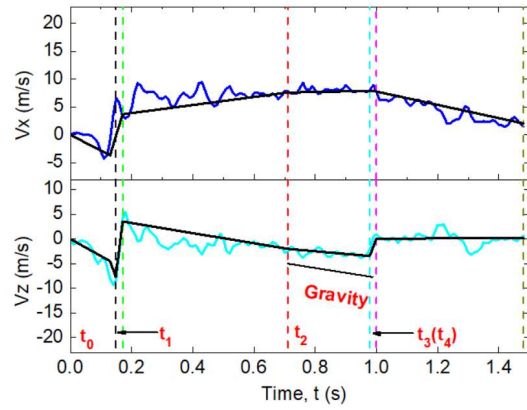
182 The vehicle contact phase has been previously well documented (Kerrigan et al., 2007; Subit et
183 al., 2008). Instead, our focus is on the subsequent ground contact. Following t_1 (first head contact on
184 the vehicle, which occurs in all tests except Test 03 where shoulder contact & low impact speed
185 prevent direct head contact), there is continued interaction of the pedestrian with the
186 bonnet/windscreen area for about 500ms until separation commences. Figure 3 shows velocity
187 changes of the head during the impact process. To aid in understanding and motivated by the
188 principle of conservation of momentum, straight line approximations of the head linear velocity have
189 been added to Figure 3, showing that no significant impacts occur between head contact on the
190 vehicle and separation from the vehicle. Following separation, the head acceleration is close to
191 gravity. Contact with the ground is predominantly vertical, with small horizontal head velocity
192 changes. Figure 4 shows the head resultant acceleration during the vehicle and ground contact
193 phases. Unfortunately, the accelerometer recording for Test 06 was corrupted during ground
194 contact. Furthermore, to address potential accelerometer vibration (mounted in the cadaver's
195 mouths using expanding foam), we employed a low-pass filter prior to injury assessments. Based on
196 previous studies (Kang and Xiao, 2008; SAE, 1995) and in order to achieve a reasonable
197 agreement between the predicted velocity changes during both vehicle and ground contact derived
198 from differentiated video positions and integrated accelerometer curves (see Appendix H), we chose
199 a CFC120 filter (3dB cut-off frequency = 200Hz), see Figure 4. With reference to Appendix H, a
200 higher or lower cut-off threshold than 200Hz resulted in respectively over/ under-prediction of the
201 velocity change compared to the video-based estimates. The significance of this approach is further
202 addressed in the Discussion.

203
204

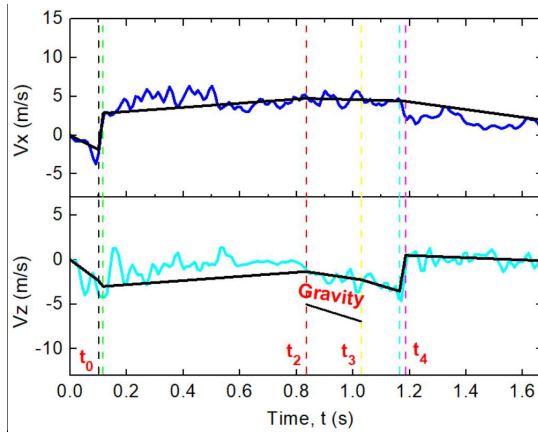
205
206
207



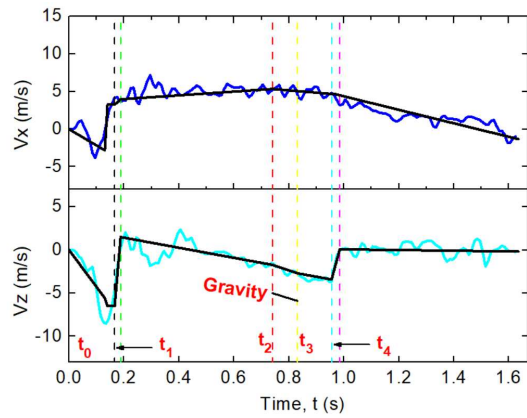
(a) Test 01



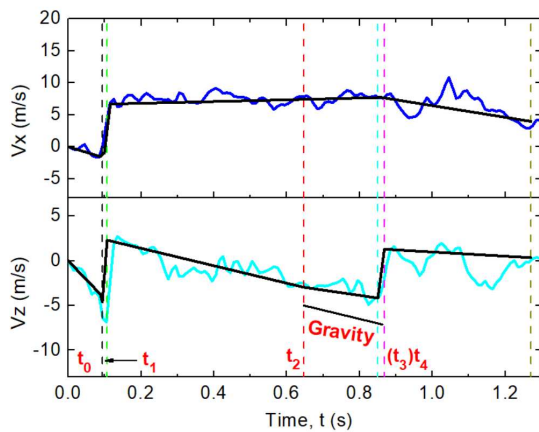
(b) Test 02



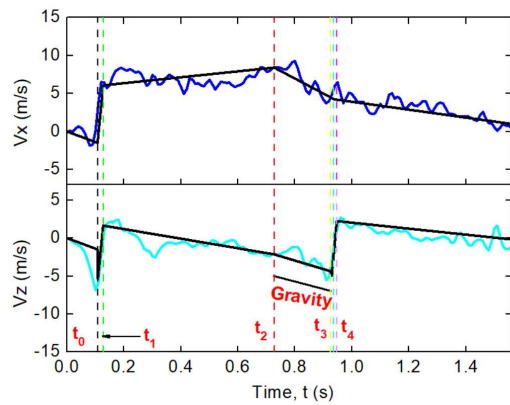
(c) Test 03



(d) Test 04



(e) Test 05



(f) Test 06

Figure 3: Head velocity time-histories from central difference (blue and cyan) with straight line approximations between major impact phases (black).

(Black dash: t_1 start; Green dash: t_1 end; Red dash: t_2 ; Yellow dash: t_3 ; Cyan dash: t_4 start; Purple dash: t_4 end)

208
209

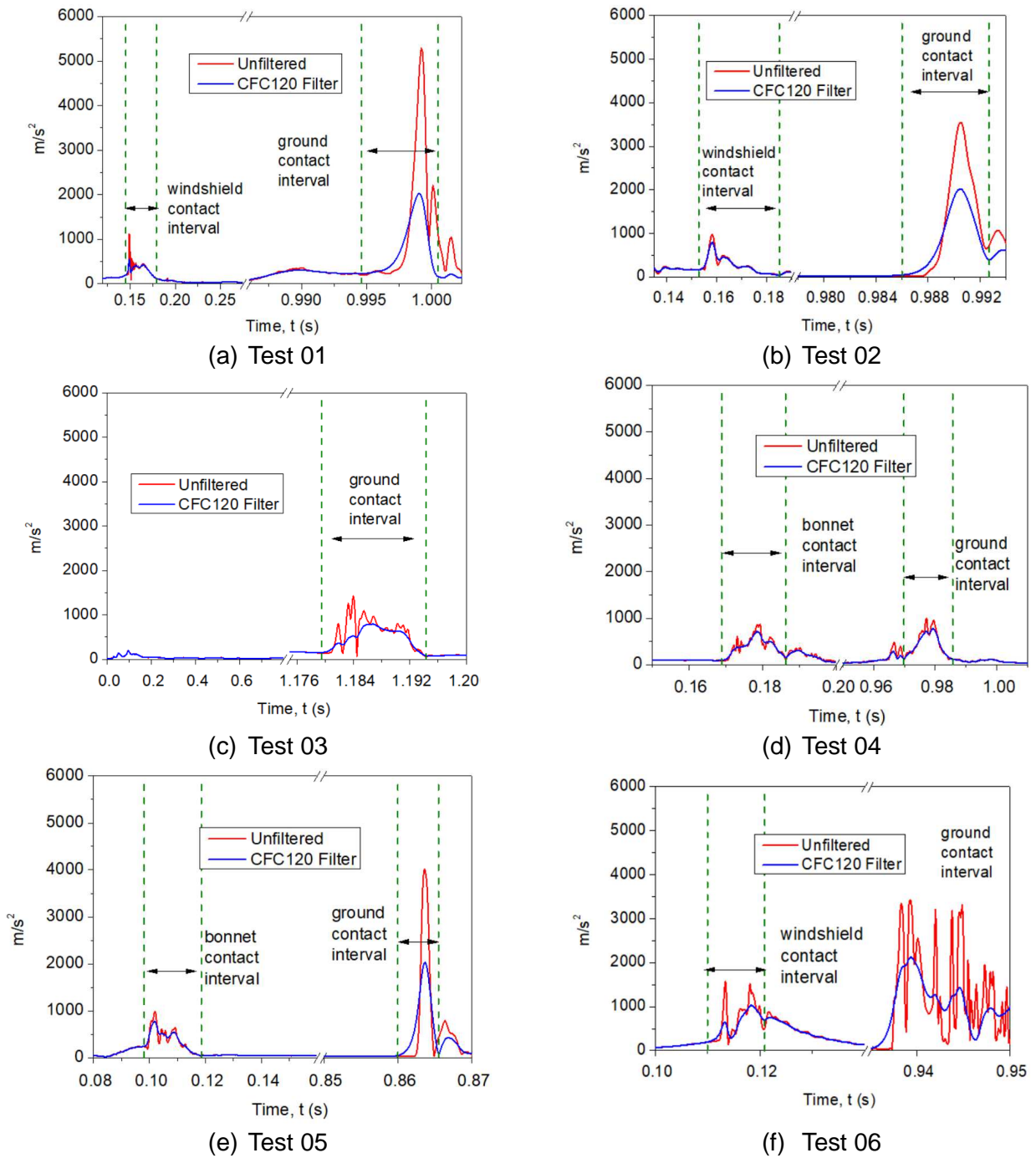


Figure 4: Filtered and unfiltered resultant head accelerometer time-histories during vehicle contact and ground contact

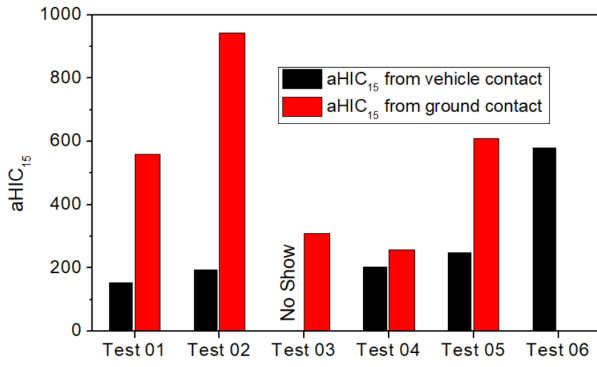
210

211

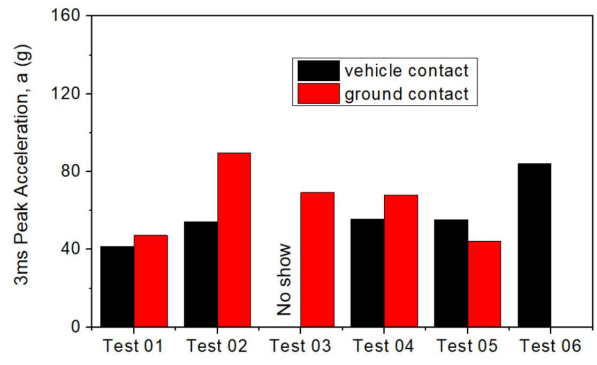
212 **3.2 Head injury risk assessments**

213 The *aHIC* scores for skull fracture risk based on the filtered acceleration curves for both vehicle
214 and ground contacts are shown in Figure 5(a)**Erreur ! Source du renvoi introuvable.** The
215 corresponding 3ms peak accelerations are shown in Figure 5(b), with head contact intervals in
216 Figure 5(c). The *BrIC* score (including the range drive from the two independent MBIM estimates)
217 and probabilities of AIS3+ brain injury risks are shown in Figures 5(d) & 5(e) respectively. A
218 comparison of the variability in computed *BrIC* and linear velocity change scores between the two
219 MBIM operators is given in Appendix I. Tables 3(a)&(b) summarize the vehicle and ground injury
220 assessments. Figure 5(f) shows average ground related rotational brain injury risk for 20km/h and
221 30km/h cases. Table 3(c) compares the expected and actual ground impact “mechanisms” using the
222 categories of (Crocetta et al., 2015), while Table 3(d) compares the corresponding head impact
223 speeds. The “agreement” in Table 3(c) is based on the proposed “mechanisms” obtained from a
224 previous simulation study (Crocetta et al., 2015). For pedestrian collisions from a compact car at 20
225 kph, almost all predicted cases were “M2”. For pedestrian collisions with a compact car or big car or
226 SUV at 30 kph, the most frequently predicted mechanism was M1. If the mechanism observed from
227 the cadaver test meets the most frequent mechanism from Crocetta et al, the “agreement” in Table
228 3(c) was categorised as “Yes”. If the observed mechanism was one of the less frequently predicted
229 ones, the agreement was “Partial”. If the observed mechanism was not predicted, then the
230 agreement was “No”.

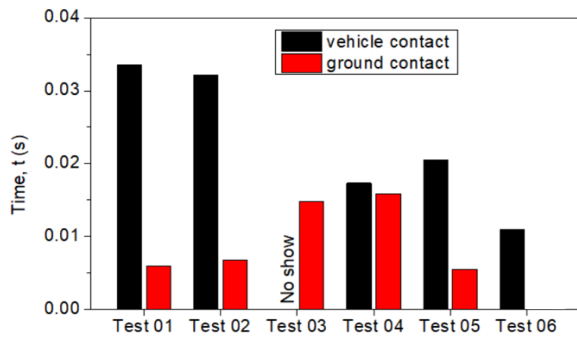
231



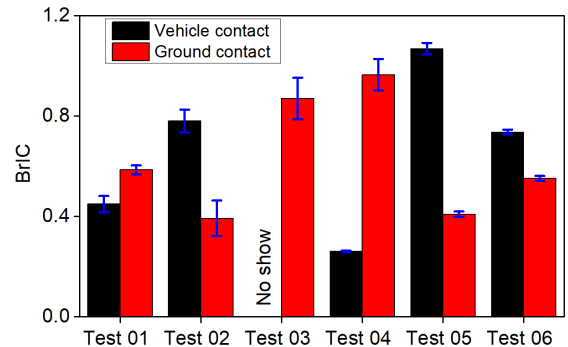
(a) Vehicle and ground related aHIC scores



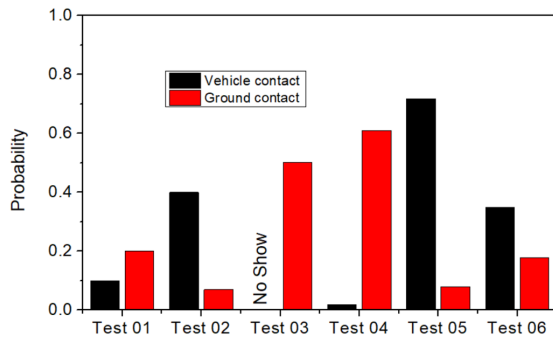
(b) The 3 ms head acceleration peaks



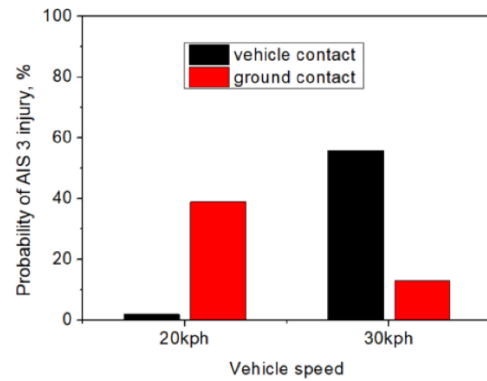
(c) Head contact intervals



(d) BrIC scores



(e) Probability of AIS3 brain injury



(f) Average ground related AIS3+ rotational brain injury risk for 20km/h and 30km/h case

Figure 5: Summary of head injuries for vehicle and ground contact

Table 3a: Summary of head/vehicle contact injury assessments

Test number	Impact speed (km/h)	NBLEH	aHIC ₁₅	3ms (g)	AIS3+ (from BrIC)
Test 01	30	0.7	152	41.5	10%
Test 02	30	0.7	194	54.4	40%
Test 03	20	0.9	---	---	--
Test 04	21	0.9	203	55.5	2%
Test 05	30	1.2	248	55.3	72%
Test 06	30	1.1	579	84.1	35%

234

Table 3b: Summary of head/ground contact injury assessments

Test number	Impact speed (km/h)	NBLEH	aHIC ₁₅	3ms (g)	AIS3+ (from BrIC)
Test 01	30	0.7	559	47	20%
Test 02	30	0.7	943	90	7%
Test 03	20	0.9	309	69	50%
Test 04	21	0.9	258	68	61%
Test 05	30	1.2	608	44	8%
Test 06	30	1.1	--	---	18%

235

Table 3c: Expected and observed pedestrian ground contact mechanisms (Crocetta et al., 2015)

Test number	Expected	Actual	Agreement
Test 01	M1 (most frequent) or M3 (less frequent)	M1	Yes
Test 02	M1 (most frequent) or M3 (less frequent)	M3	Partial
Test 03	M2	M2	Yes
Test 04	M2	M2	Yes
Test 05	M2 (most frequent) or M1 (less frequent)	M1	Partial
Test 06	M2 (most frequent) or M1 (less frequent)	M1	Partial

236

Table 3d: Expected and observed ground contact speeds (Crocetta et al., 2015)

Test number	Cadaver head velocity (m/s) at ground contact	Average \pm std dev. head velocity (m/s) at ground contact from multibody predictions (Crocetta et al., 2015)
Test 01	5.1	4.7 \pm 0.8
Test 02	2.6	2.9 \pm 0.6
Test 03	5.1	3.2 \pm 1.4
Test 04	3.9	3.2 \pm 1.4
Test 05	4.4	4.7 \pm 0.8
Test 06	5.5	4.7 \pm 0.8

237

239 **4.Discussion**

240 ***Whole-body kinematics during the complete pedestrian impact process***

241 We present the first detailed overview of the kinematic process of pedestrian ground contact
242 using cadavers (see Table 2 and Figure 2). The very limited previous data on pedestrian ground
243 contact from cadaver tests limits comparison to the published literature. Whole body kinematics can
244 be classified into several critical events and phases: phase 1 (duration ~100-170ms) starts with first
245 pedestrian-vehicle contact and ends with first head-vehicle contact; in phase 2 (duration ~550-
246 625ms) the pedestrian moves together with the vehicle; phase 3 (duration ~185-280ms) is
247 separation and first pedestrian ground contact; phase 4 (duration ~1-1.8s) is slide, roll and bounce
248 to rest. First head ground contact occurs after about 1s and the process is complete after about 2.0-
249 2.8s. Pedestrian ground contact occurs at the end of a highly non-linear chain of events, such that
250 small changes in initial configuration result in significant changes in head ground impacts (compare
251 Test 01 to Test 02) and this has been well flagged in the literature (Simms and Wood, 2009).
252 However, considering the ground contact “mechanisms” proposed by (Crocetta et al., 2015) – see
253 Appendix C, surprisingly good agreement was observed (Table 3c) and head velocity prior to ground
254 contact was similar to the range presented for each mechanism except for Test 03 (Table 3d). These
255 results show multibody modelling is generally successful at predicting whole body motion of
256 pedestrians during ground contact. Nonetheless, given variations in head ground impact observed
257 in similar cadaver tests (especially Test 01 vs Test 02), the capacity to predict injury risk in specific
258 ground contact cases is low, as per modelling observations (Li et al., 2017b).

259 ***Head kinematics throughout the impact process***

260 Head velocity changes (Figure 3) clearly identify the head/vehicle and head/ground contact
261 processes. It is instructive to conceive of the head velocity changes in terms of net forces acting
262 vertically and horizontally: the horizontal head velocity changes in phase 1 are due to neck forces
263 induced during body rotation. Then there is the vehicle contact, after which the horizontal velocities
264 during phases 2 and 3 are largely constant (almost zero net force) during separation from the
265 vehicle through to first pedestrian ground contact, after which sliding and rolling to rest during phase
266 4 reduce the horizontal velocity to zero. The vertical head velocity changes in phase 1 are again due
267 to neck forces induced by body rotation. Then there is the vehicle contact, after which the vertical
268 velocity changes approximately follow gravity during separation from the vehicle through to first
269 pedestrian ground contact, which again effectively reduces the vertical component of head velocity
270 to zero.

271 ***Head ground contacts***

272 The cadavers mostly struck the ground after around 1s (Test 05 was earlier but in this case
273 there was an unusually low subject mass). The head impacts the ground more than once in each
274 test, indicating significant restitution. However, estimates of head/ground contact stiffness using a
275 spring-mass model with restitution were variable, between ca. 180-1750 kN/m, see Appendix J.
276 Figure 3 shows that ground contact is predominantly vertical, with small horizontal velocity change
277 during ground impact in all six tests. In contrast, the vertical velocity change during ground contact
278 is chiefly responsible for the acceleration peaks in Figure 4. The peak accelerations, a_{HIC} and $3ms$

279 scores from ground contact are generally higher than those from vehicle contact, see Figure 5. The
 280 high stiffness of the ground contact evidenced by the shorter contact interval compared to the
 281 vehicle contact (Figure 5c) is probably the main reason for this, since Appendix H shows the speed
 282 change in the vehicle contacts is mostly higher than in the ground contacts. This highlights the need
 283 to find solutions to pedestrian ground contact injury for pedestrian protection at impact speeds of 20
 284 - 30 km/h, where further improvements in vehicle front safety may be less beneficial than
 285 approaches to preventing pedestrian ground contact. These results are in line with our recent
 286 GIDAS analysis which found 72% of injury costs in pedestrian collisions below 30km/h are
 287 associated with ground related injuries (Shang et al., 2018b).

288 **Head accelerometer filtering**

289 According to the X-ray after each test, there were no skull fractures. This provides further
 290 justification for the 200 Hz filter, as the peaks in the unfiltered accelerations in Figure 4 would almost
 291 certainly imply some skull fractures. In addition, a retrospective assessment of the GIDAS data
 292 analyzed for the work published in (Shang et al., 2018b) shows the proportion of crashes involving
 293 skull fracture from ground contact is less than 4% in the speed range 25-34 km/h and less than 1%
 294 in the speed range 15-34 km/h, which also complies with the absence of skull fractures in our
 295 cadaver tests.

296 **Head linear versus rotational loading during ground contact**

297 A comparison of the relationship between *aHIC*/3ms linear head injury risk with the rotationally
 298 assessed AIS3+ risk computed from the *BrIC* score shows mixed results, see Figure 6. The *aHIC*
 299 score reduces with increased AIS3+ rotational head injury risk suggesting a compensatory pattern
 300 between head linear and angular injury risk which might depend on the geometry of head ground
 301 contact, but this pattern is not replicated for the 3ms score. It is thus unclear how to interpret these
 302 results and computational modelling may be needed to further elucidate this.

303

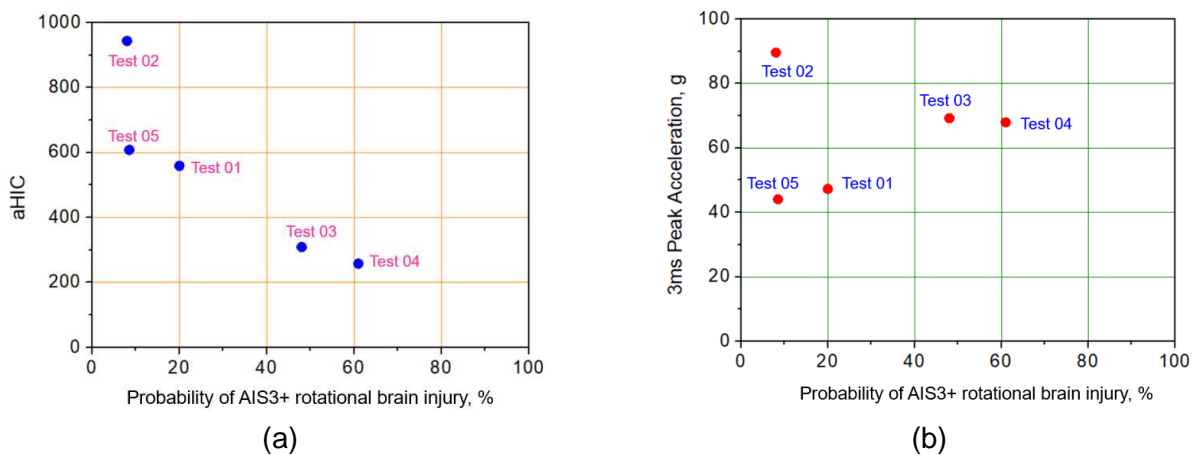


Figure 6: Comparison of the relationship between *aHIC*/3ms linear head injury risk with the rotationally assessed AIS3+ risk for Test 01-05 (the accelerometer malfunctioned in the ground contact in Test 06)

304 **Unexpected Results**

305 There were a number of unexpected findings that may lead to future insights:

306 Figure 5(f) and Table 3b show a substantially higher risk of rotationally induced brain injury for the
307 two 20 km/h tests than the four 30 km/h cases. The reason for this is the combination of a larger
308 ω_z component with the smaller threshold for this axis in the BrIC equation. By checking the head-
309 ground contact mechanisms from the videos, the motion of the pedestrian heads in tests 03 and 04
310 was more complex (bending and twisting). In contrast, for the other tests, the heads showed mainly
311 bending rotation during contact with the ground. An underlying biomechanical explanation and
312 whether this predicted increased risk at 20kph occurs in real world collisions remains unclear, but
313 future computational modelling may help elucidate this.

314 We had expected to identify a relationship between NBLEH and head injury risk as this was
315 observed in our recent analysis of GIDAS data (Shang et al., 2018b), but Table 3a shows no clear
316 relationship between either linear or rotational head injury risk assessments in ground contact and
317 the NBLEH in our cadaver tests. The absence of a trend may be due to the small sample size.
318

319 **5. Limitations**

320 A larger sample size would be needed to better understand the influence of vehicle design and
321 pedestrian ground contact. However, the current experimental findings could be combined with
322 computational modelling to better understand these effects. Additional high-speed cameras and
323 markers on the head would have been beneficial for the MBIM process, as the region of interest to
324 be covered during the whole process from first contact to rest is large.

325 The CFC 120 filter applied to the accelerations gave the closest speed change by comparison
326 with the MBIM data than any other filter we investigated, and we therefore believe it is appropriate
327 to apply this filter setting. However, we acknowledge this filter not only reduces the peak but can
328 also slightly change the contact time defined, see Figure 4. In future, a study dedicated to
329 establishing appropriate filters for pedestrian ground contact would be helpful.

330 The accuracy of the angular velocity time histories derived from the MBIM process cannot be
331 measured as there is no gold standard, and this is a limitation. However, compared to (Tierney et
332 al., 2018), we expect a higher accuracy as the frame rate is higher and there are four cameras
333 instead of three and the image resolution is better. The intraclass correlation coefficients for the
334 results of the two independent researchers applying MBIM are given in Table I.1. An assessment of
335 rotationally induced brain injury which includes a measure of angular acceleration would be
336 preferable, however, unfortunately we were not able to estimate angular acceleration in this study
337 due to limitations in the available sensors. Furthermore, we recognise the limitations of BrIC which
338 include a lack of validation data and its possible weakness for predicting more severe injuries.

339 A nine accelerometer array suitable for computing head CG accelerations would have permitted
340 more precise 3ms, HIC calculations and would also facilitate UBrIC computation. A method for
341 enforcing known initial limb angles would be beneficial, but also difficult to achieve in these cadaver
342 tests. Furthermore, the cadavers' lack of muscle tone may result in different kinematics compared to
343 live pedestrians, especially for the two 20 kph tests. In this paper only head kinematics are
344 presented, but the GIDAS data (Shang et al., 2018b) shows lower limb and spinal injuries also
345 occur during pedestrian ground contact and these should be a focus of future work.

346 **6. Conclusions**

347 This paper presents the first detailed analysis of pedestrian ground contact kinematics using
348 staged cadaver tests addressing a range of vehicle shapes and pedestrian heights and impact
349 speeds of 20 and 30 km/h. In addition to the well-established kinematics of pedestrians up to the
350 time of head contact on the vehicle, we have observed around 500 ms of continued interaction of
351 the pedestrian on the vehicle until separation commences, followed by a flight period of around 200
352 ms which terminates in ground contact. The linear accelerations in ground contact for vehicle impact
353 speeds of 20 and 30 km/h are generally higher than the acceleration in the vehicle contact, though
354 the contact intervals are shorter. No skull fractures were observed in any cases, but the 3ms scores
355 are close to or above the injury threshold in several cases. The predicted risk of rotationally induced
356 brain injury computed from model based image matching applied to ground contact is high for the
357 20 km/h tests, highlighting the risk of pedestrian injuries from ground contact even at very low
358 speeds. We were unable to identify a clear relationship between vehicle shape/pedestrian height
359 and ground contact head injury risk in these six tests. The data pertaining to these six pedestrian
360 ground contact tests can be made available upon request for the purpose of human body model
361 development.

362 **Conflict of Interest**

363 The authors have no conflict of interest related to the present work to disclose.

364 **Acknowledgement**

365 The support of the China Scholarship Council (CSC) is highly appreciated.
366

367 **References**

368
369 Aomura, S., Zhang, Y., Nakadate, H., Koyama, T., Nishimura, A., 2016. Brain injury risk estimation of
370 collegiate football player based on game video of concussion suspected accident. *Journal of Biomechanical*
371 *Science*
372 *Engineering* 11, 16-00393-00316-00393.
373 Ashton, S., Mackay, G., 1983. Benefits from changes in vehicle exterior design—field accident and
374 experimental work in Europe. SAE Technical paper.
375 Badea-Romero, A., Lenard, J., 2013. Source of head injury for pedestrians and pedal cyclists: Striking vehicle
376 or road? *Accident Analysis & Prevention* 50, 1140-1150.
377 Bahr, R., Krosshaug, T., 2005. Understanding injury mechanisms: a key component of preventing injuries in
378 sport. *British Journal of Sports Medicine* 39, 324-329.
379 Cavallero, C., Cesari, D., Ramet, M., Billault, P., Farisse, J., Seriat-Gautier, B., Bonnoit, J., 1983. Improvement
380 of pedestrian safety: influence of shape of passenger car-front structures upon pedestrian kinematics and
381 injuries: evaluation based on 50 cadaver tests. SAE Technical Paper.
382 Crocetta, G., Piantini, S., Pierini, M., Simms, C., 2015. The influence of vehicle front-end design on pedestrian
383 ground impact. *Accident Analysis & Prevention* 79, 56-69.
384 ECE, 2008. Regulation No 21 of the Economic Commission for Europe of the United Nations (UN/ECE) —
385 Uniform provisions concerning the approval of vehicles with regard to their interior fittings.
386 ECE, 2010. Regulation No 25 of the Economic Commission for Europe of the United Nations (UN/ECE) —

387 Uniform provisions concerning the approval of head restraints (headrests), whether or not incorporated in
388 vehicle seats.

389 Gabler, L.F., Crandall, J.R., Panzer, M.B., 2016. Assessment of kinematic brain injury metrics for predicting
390 strain responses in diverse automotive impact conditions. *Annals of Biomedical Engineering* 44, 3705-3718.

391 Gabler, L.F., Crandall, J.R., Panzer, M.B., 2018. Development of a metric for predicting brain strain responses
392 using head kinematics. *Annals of Biomedical Engineering* 46, 972-985.

393 Goodarzi, N., Akbari, G., Razeghi Tehrani, P., 2017. Zinc Chloride, A new material for embalming and
394 preservation of the anatomical specimens. *Anatomical Sciences Journal* 14, 25-30.

395 Got, C., Patel, A., Fayon, A., Tarriere, C., Walfisch, G., 1978. Results of experimental head impacts on
396 cadavers: the various data obtained and their relations to some measured physical parameters. SAE
397 Technical Paper.

398 Gupta, V., Kalra, A., Shen, M., Chou, C.C., Yang, K.H., 2015. Effect of vehicle front end profile on pedestrian
399 kinematics and biomechanical responses using a validated numerical model, ASME 2015 International
400 Mechanical Engineering Congress and Exposition. American Society of Mechanical Engineers.

401 Gupta, V., Yang, K.H., 2013. Effect of vehicle front end profiles leading to pedestrian secondary head impact
402 to ground. SAE Technical Paper.

403 Hamacher, M., Eckstein, L., Kühn, M., Hummel, T., 2011. Assessment of active and passive technical
404 measures for pedestrian protection at the vehicle front, 22st International Technical Conference on the
405 Enhanced Safety of Vehicles (ESV 2011).

406 Han, Y., Li, Q., Wang, F., Wang, B., Mizuno, K., Zhou, Q., 2018. Analysis of pedestrian kinematics and ground
407 impact in traffic accidents using video records. *International Journal of Crashworthiness*, 1-10.

408 Hutchinson, J., Kaiser, M.J., Lankarani, H.M., 1998. The head injury criterion (HIC) functional. *Applied
409 Mathematics Computation* 96, 1-16.

410 Kalra, A., Gupta, V., Shen, M., Jin, X., Chou, C.C., Yang, K.H., 2016. Pedestrian safety: an overview of
411 physical test surrogates, numerical models and availability of cadaveric data for model validation. *International
412 Journal of Vehicle Safety* 9, 39-71.

413 Kang, S., Xiao, P., 2008. Comparison of Hybrid III rigid body dummy models, 10th International LSDYNA
414 Users Conference.

415 Kendall, R., Meissner, M., Crandall, J., 2006. The causes of head injury in vehicle-pedestrian impacts:
416 comparing the relative danger of vehicle and road surface. SAE Technical paper.

417 Kerrigan, J.R., Crandall, J.R., Deng, B., 2007. Pedestrian kinematic response to mid-sized vehicle impact.
418 *International Journal of Vehicle Safety* 2, 221-240.

419 Kimpara, H., Iwamoto, M., 2012. Mild traumatic brain injury predictors based on angular accelerations during
420 impacts. *Annals of Biomedical Engineering* 40, 114-126.

421 Li, G., Lyons, M., Wang, B., Yang, J., Otte, D., Simms, C., 2017a. The influence of passenger car front shape
422 on pedestrian injury risk observed from German in-depth accident data. *Accident Analysis & Prevention* 101,
423 11-21.

424 Li, G., Yang, J., Simms, C., 2017b. Safer passenger car front shapes for pedestrians: A computational
425 approach to reduce overall pedestrian injury risk in realistic impact scenarios. *Accident Analysis & Prevention*
426 100, 97-110.

427 Masson, C., Serre, T., Cesari, D., 2007. Pedestrian-vehicle accident: Analysis of 4 full scale tests with PMHS,
428 20th International Technical Conference on the Enhanced Safety of Vehicles (ESV) National Highway Traffic
429 Safety Administration.

430 Mueller, B., MacAlister, A., Nolan, J., Zuby, D., 2015. Comparison of HIC and BrIC head injury risk in IIHS

431 frontal crash tests to real-world head injuries, Proceedings of the 24th International Technical Conference on
432 the Enhanced Safety of Vehicles.

433 Niebuhr, T., Junge, M., Rosén, E., 2016. Pedestrian injury risk and the effect of age. *Accident Analysis &*
434 *Prevention* 86, 121-128.

435 Paas, R., Masson, C., Davidsson, J., 2015. Head boundary conditions in pedestrian crashes with passenger
436 cars: six-degrees-of-freedom post-mortem human subject responses. *International Journal of*
437 *Crashworthiness* 20, 547-559.

438 Rosen, E., Stigson, H., Sander, U., 2011. Literature review of pedestrian fatality risk as a function of car
439 impact speed. *Accident Analysis & Prevention* 43, 25-33.

440 SAE, 1995. Instrumentation for impact test—Part 1—Electronic instrumentation. SAE 211.

441 Schmitt, K.-U., Niederer, P., Muser, M., Walz, F., 2010. *Trauma Biomechanics*. Springer.

442 Shang, S., Li, G., Otte, D., Simms, C., 2018a. An inverse method to reduce pedestrian - ground contact
443 injuries IRCOBI Asia 2018.

444 Shang, S., Otte, D., Li, G., Simms, C., 2018b. Detailed assessment of pedestrian ground contact injuries
445 observed from in-depth accident data. *Accident Analysis & Prevention* 110, 9-17.

446 Simms, C., 2005. Sports utility vehicles and older pedestrians. *BMJ* 331, 787.

447 Simms, C., Wood, D., 2009. *Pedestrian and Cyclist Impact*. Springer Netherlands.

448 Subit, D., Kerrigan, J., Crandall, J., Fukuyama, K., Yamazaki, K., Kamiji, K., Yasuki, T., 2008. Pedestrian-
449 vehicle interaction: kinematics and injury analysis of four full scale tests, Proceedings of IRCOBI Conference,
450 pp. 275-294.

451 Takhounts, E.G., Craig, M.J., Moorhouse, K., McFadden, J., Hasija, V., 2013. Development of brain injury
452 criteria (BrIC). SAE Technical Paper.

453 Tamura, A., Duma, S., 2011. A study on the potential risk of traumatic brain injury due to ground impact in a
454 vehicle-pedestrian collision using full-scale finite element models. *International Journal of Vehicle Safety* 5,
455 117-136.

456 Tamura, A., Koide, T., Yang, K.H., 2014. Effects of ground impact on traumatic brain injury in a fender vault
457 pedestrian crash. *International Journal of Vehicle Safety* 8, 85-100.

458 Taneda, K., Kondo, M., Higuchi, K., 1973. Experiment on passenger car and pedestrian dummy collision,
459 Proceedings of the International Research Council on the Biomechanics of Injury conference. International
460 Research Council on Biomechanics of Injury, pp. 231-239.

461 Tierney, G., Krosshaug, T., Wilson, F., Simms, C., 2015. An assessment of a novel approach for determining
462 the player kinematics in elite rugby union players, Proceedings of the International Research Council on
463 Biomechanics of Injury, pp. 180-181.

464 Tierney, G.J., Joodaki, H., Krosshaug, T., Forman, J.L., Crandall, J.R., Simms, C.K., 2018. Assessment of
465 model-based image-matching for future reconstruction of unhelmeted sport head impact kinematics. *Sports*
466 *Biomechanics* 17, 33-47.

467 Versace, J., 1971. A review of the severity index. SAE Technical Paper.

468 WHO, 2013. Global status report on road safety 2013: supporting a Decade of Action. World Health
469 Organization.

470 Winckler, G., 1974. *Manuel d'anatomie topographique et fonctionnelle*. Masson.

471 Xu, J., Shang, S., Yu, G., Qi, H., Wang, Y., Xu, S., 2016. Are electric self-balancing scooters safe in vehicle
472 crash accidents? *Accident Analysis & Prevention* 87, 102-116.

473

Table A.1-1 External anthropometry

Anthropometry	Test 01	Test 02	Test 03	Test 04	Test 05	Test 06
1 total height	174	172	167	167	157	163
2 eyes / ground height	166	161	162	155	147	153
3 acromion / ground height	149	144	145	137	121	141.5
4 elbow / ground height	116	110	109	106	97	110
5 iliac spine / ground height	95	94	91	91	84	95
6 trochanter / ground height	88	89	82	86	78	89.5
7 hauteur interligne genoux/sol	46	46	45	44.5	42	49
43 ankle height	6	8	7	10	5	8.5
44 a arm high circumference	27.5	31.5	31	25.3	18	28.5
44 b arm low circumference	26	28	28	24	17.5	27
48 a forearm high circumference	27	24	28.5	25	16.3	25.7
48 b forearm low circumference	19	19	20	19	12.5	18
49 hand length	20	18	19	18	13	20
36 thigh high circumference	42	46	46.5	40.5	33.5	47.5
37 thigh low circumference	35.5	38	39	36	27	39.5
38 knee circumference	37.5	38	36.5	37.5	33	37
39 calf circumference	30.5	31	29.5	30.5	20	29
40 ankle circumference	26	25	26.5	26.5	22.5	25
41 foot width	10	10	10.5	10.5	7	85
42 foot length	27.5	27	26.5	22.5	20	23
10 shoulder width	43	48	39.5	40.5	28.5	36
20 axillary thoracic width	36	35	31	39	27	34
23 thorax width under sternum	35	34	31	31.5	24	31

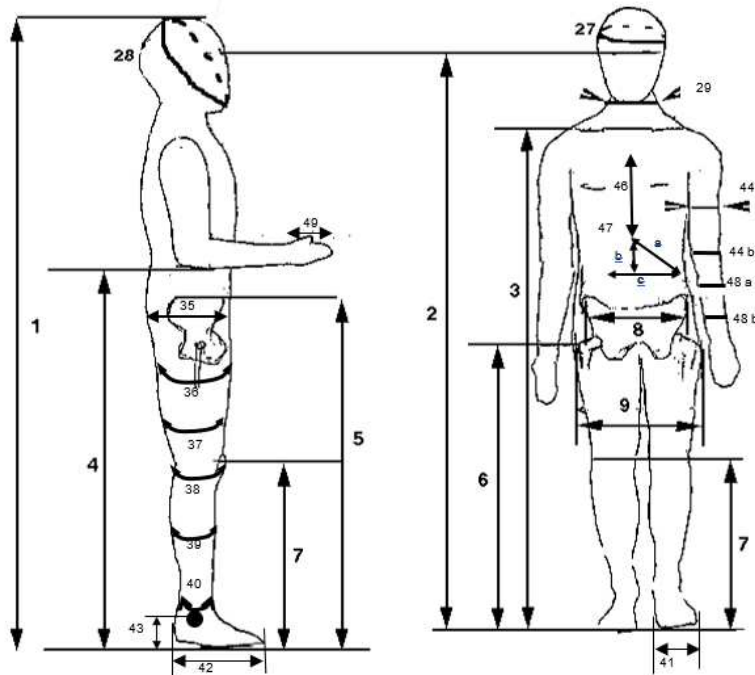
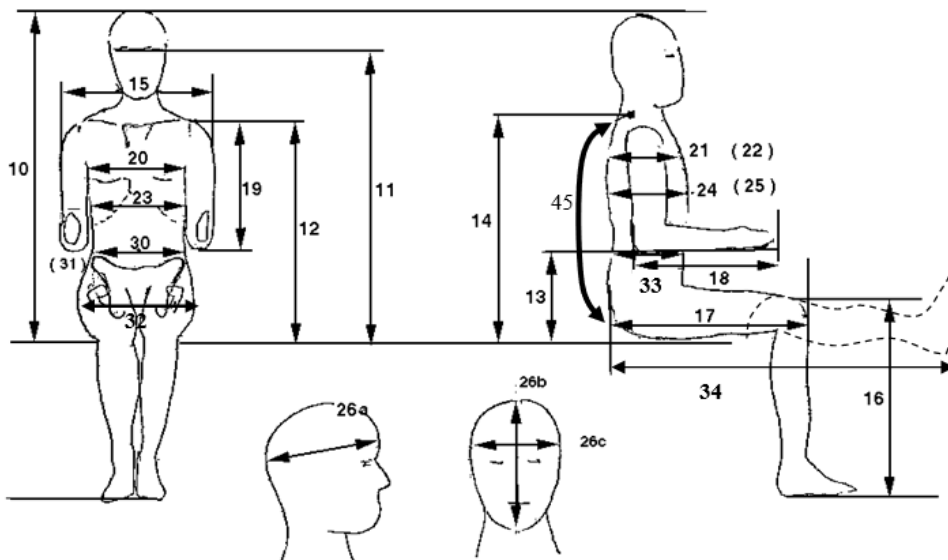


Table A.1-2 External anthropometry (continued)




Anthropometry	Test 01	Test 02	Test 03	Test 04	Test 05	Test 06
30 abdomen width	37	36	29	37	26	33
8 pelvis width	35	35	26.5	26	26.5	28
9 bi-trochanter width	39	36	39	33	27	36
21 thoracic axillary thickness	27	22	23	12	9	12
24 thoracic thickness under sternum	-	22	18	18	15	21
33 abdomen thickness	18	17	17	14	25.5	21
35 buttocks thickness	16	17	19	14	12	15
26a head / forehead depth	26	21	19	18	16	18
26b head height	28	23.5	20	21.5	20	23
26c head width	17.5	18	16	14	12	15
27 head circumference	55.5	58	56	56	52	56.5
28 chin-occipital circumference	72	69	63	59	62	61
29 neck circumference	41.5	48	40.5	39	33.5	48
18 forearm + hand length	46	44	37	41.5	34	44.5
19 arm length	33.5	32	32	32	26	30
10 seat height	98	88	85	92	72	85
11 eyes / seat height	90	77	80	83	62	75
14 cervical / seat height	79	70	70	68	55	67
12 acromion / seat height	73	60	63	65	48	63.5
13 elbow / seat height	40	16	27	33	26	37
22 axillary thoracic circumference	93	104	93	89	79	98
25 thoracic circumference under sternum	85	93	87.5	75	77	101
31 abdominal circumference (navel)	83	88	78	75	78	91
32 pelvis circumference	88	94	90	87	72	96
16 knee / ground height	46	51	51	43	41	48
17 buttocks / knee length	40.5	52	38	30	35	29
34 pelvis / heel (stretched leg) length	88	93	93	82	78	97.5
45 T1 – coccyx length	75	68	65	-	47	64
46 sternum length	17	19	19	22	19	20
47 xiphoid angle (a, b, c)	16 17 20	20 12 25	19 10 26	17 7 34	13 7 23	20 13 33



482 **Appendix B: Vehicles used**

483

Table B1: Vehicles used

Vehicle model	Pictures of vehicle	Partly parameters of vehicle
(a) Peugeot 307		Vehicle Height: 1510 mm Windshield Angle: 25.8° Bonnet Angle: 16.2° Bonnet length: 730 mm
(b) Citroen C4		Vehicle Height: 1491 mm Windshield Angle: 25.3° Bonnet Angle: 8.2° Bonnet length: 820 mm
(c) Renault Kangoo II		Vehicle Height: 1844 mm Windshield Angle: 38.4° Bonnet Angle: 8.2° Bonnet length: 540 mm

484

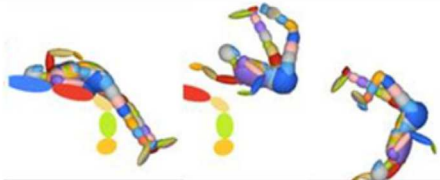

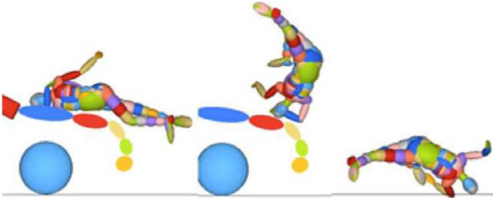
485

486

487 **Appendix C: Ground contact “mechanisms”**

488

Table C1: Expected ground contact mechanisms (Crocetta et al., 2015)

Description	Kinematics
M1: wrap trajectory - pedestrian rotates 90°-180° before impacting ground head first	
M2: wrap trajectory - pedestrian rotates 0°-90° before impacting ground pelvis first, then head	
M3: wrap trajectory - pedestrian rotates 180°-270° before impacting ground head first	

489

490

491 **Appendix D: Camera layout used**

492

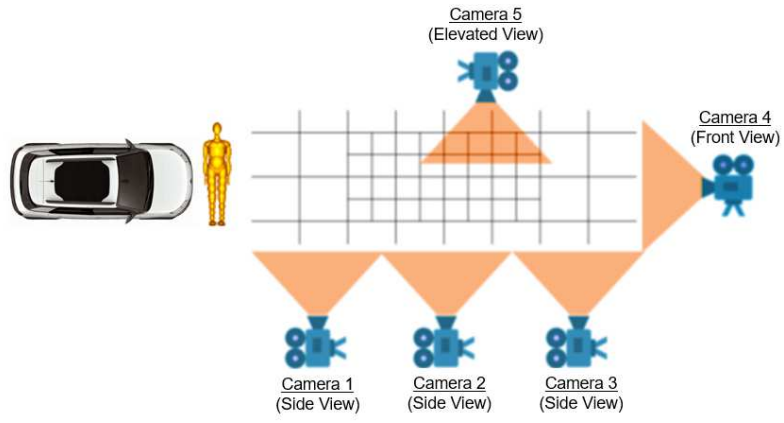


Figure D1: The general locations of the high-speed cameras

493

494

495

496
497

Appendix E: Lower limb initial joint angles estimates

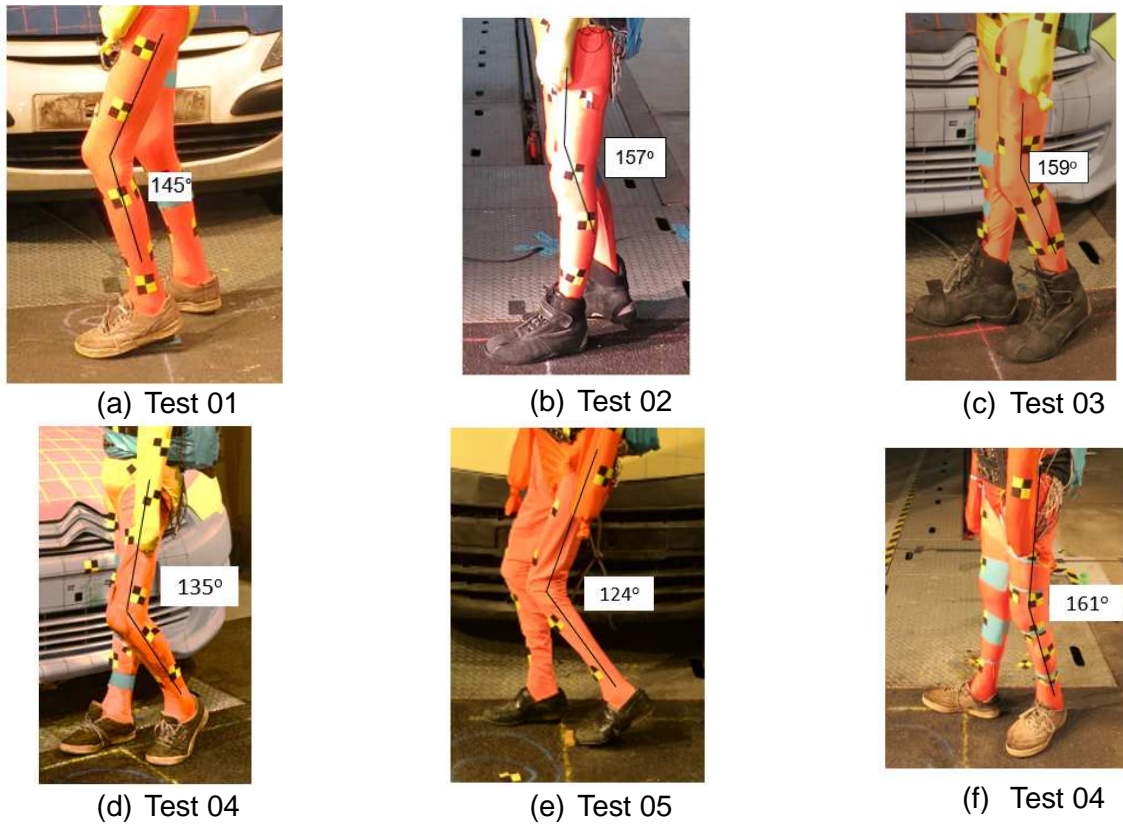
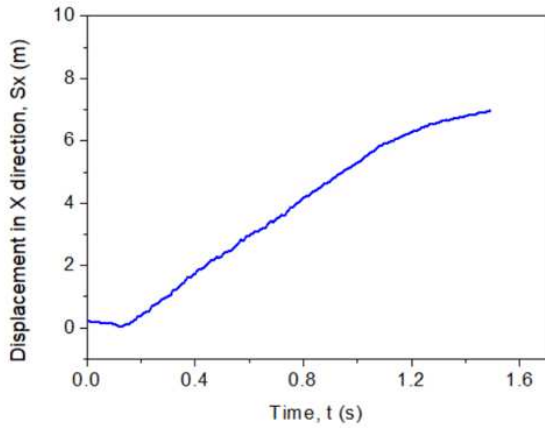


Figure E1: Knee joint angles in pre-impact positions

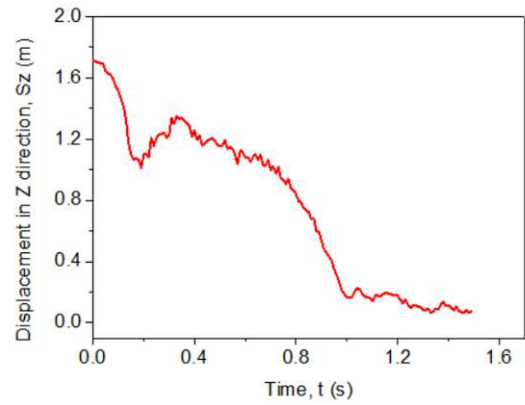
498
499
500

501 **Appendix F: Head marker trajectories in tests**

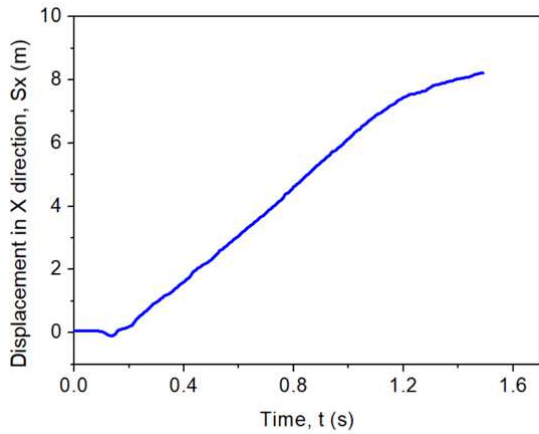
502



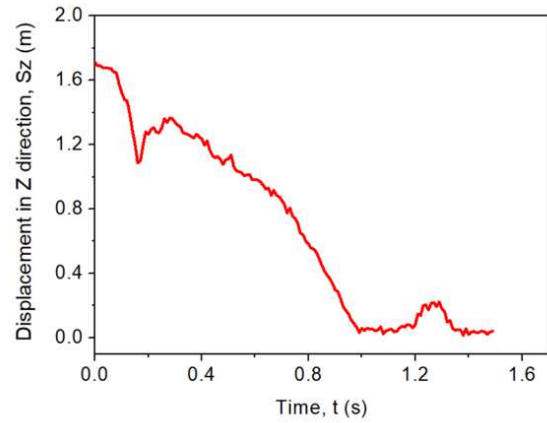
(a) Head position in X direction for Test 01



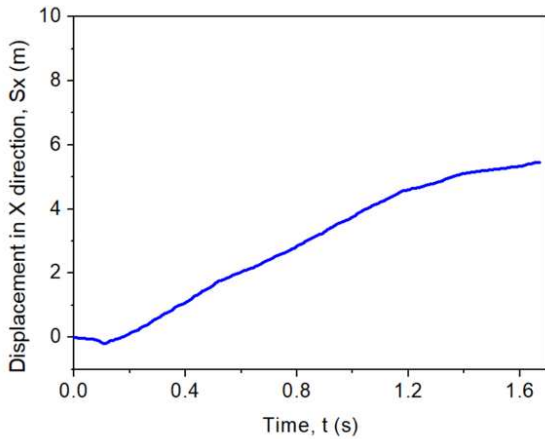
(b) Head position in Z direction for Test 01



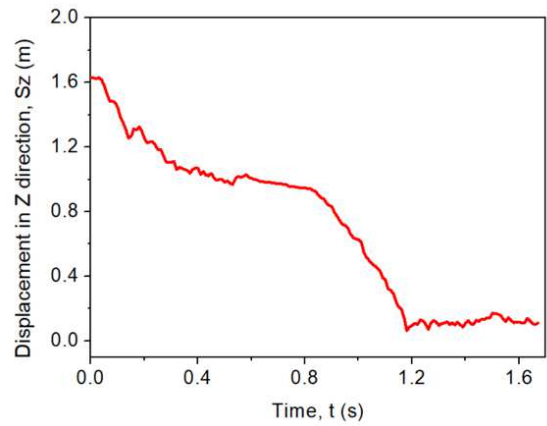
(c) Head position in X direction for Test 02



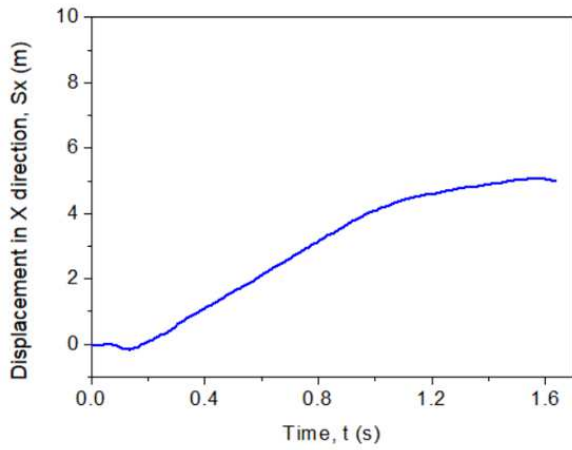
(d) Head position in Z direction for Test 02



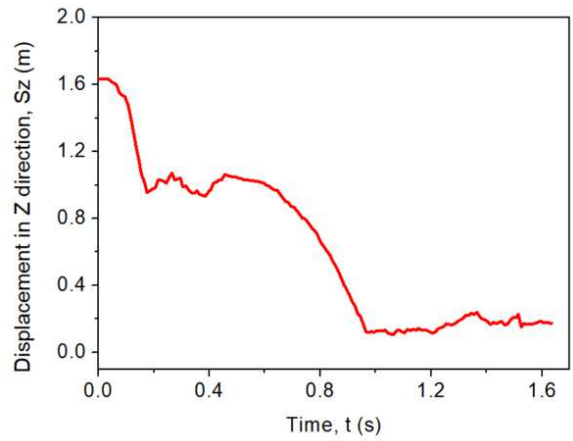
(e) Head position in X direction for Test 03



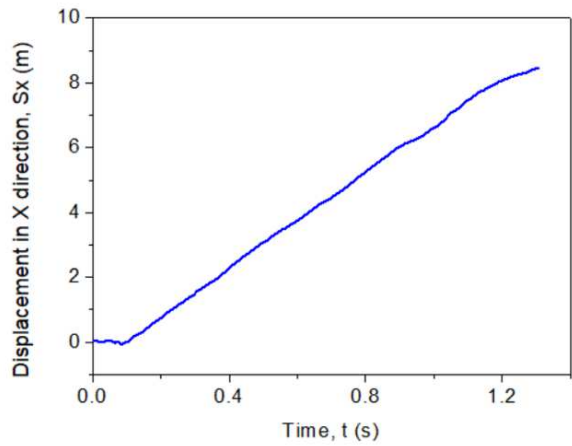
(f) Head position in Z direction for Test 03



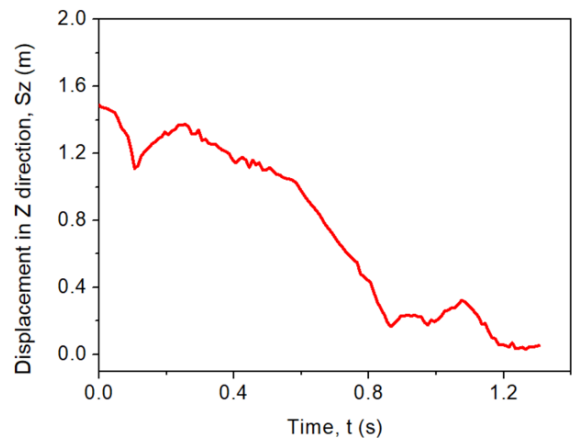
(g) Head position in X direction for Test 04



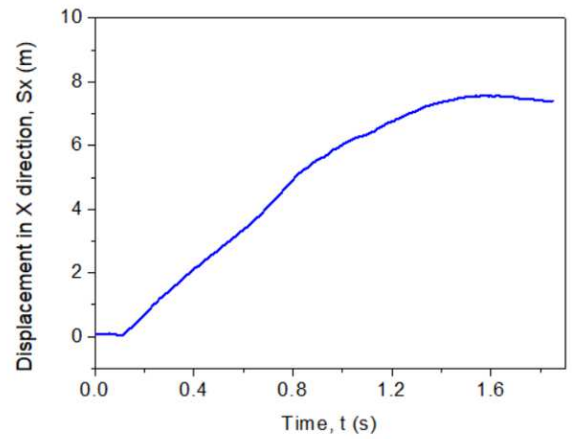
(h) Head position in Z direction for Test 04



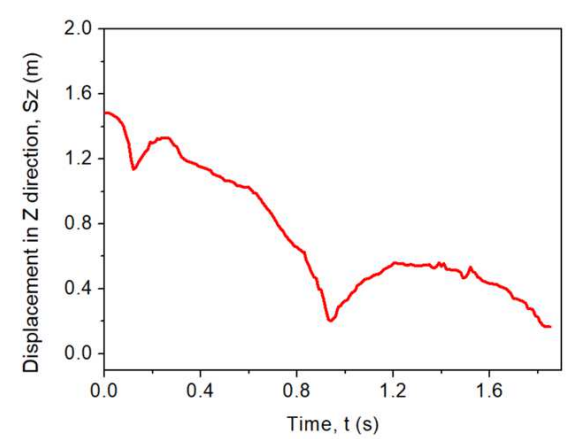
(i) Head position in X direction for Test 05



(j) Head position in Z direction for Test 05



(k) Head position in X direction for Test 06



(l) Head position in Z direction for Test 06

Figure F1: Cadaver head displacement in X and Z directions for the six tests

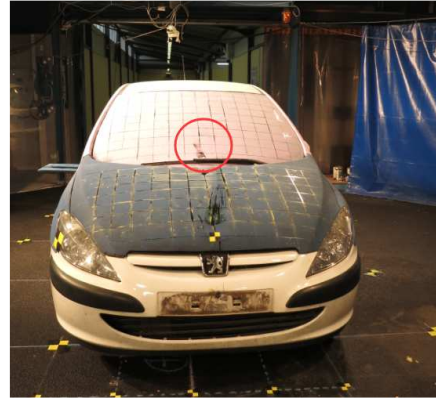
503
504
505

506 **Appendix G: Head impact location on vehicle**

507

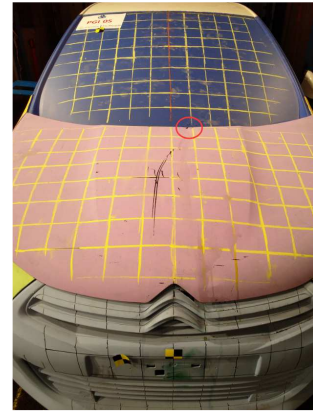


(a) Test 01



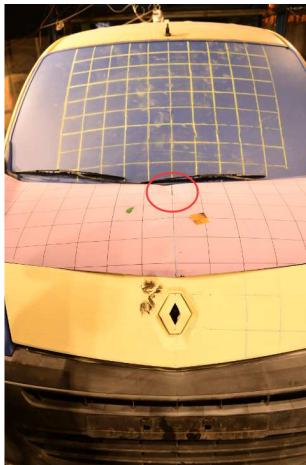
(b) Test 02

No head contact

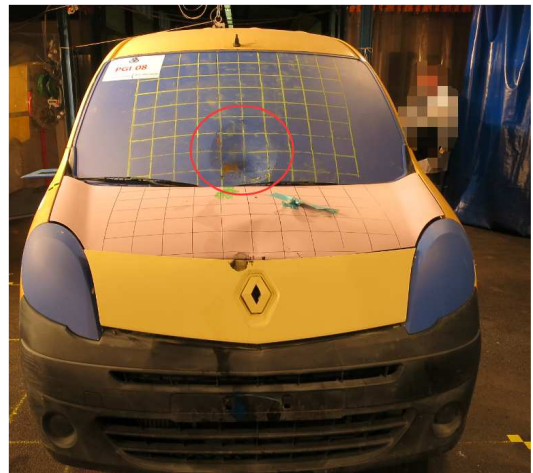


(d) Test 04

(c) Test 03



(e) Test 05



(f) Test 06

Figure G1: Pedestrian head impact location on vehicle

508

509 **Appendix H: Head resultant velocity change during vehicle and ground contacts from video**
510 **data differentiation and accelerometer integration**
511

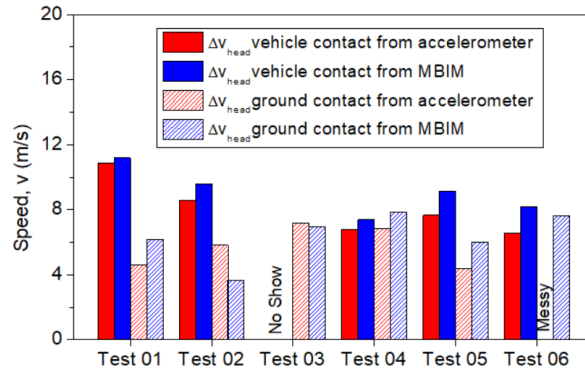


Figure H1: Comparison of head speed changes from MBIM and accelerometer

512

513

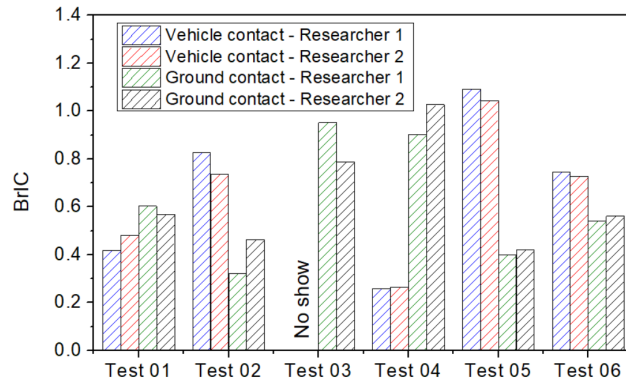


Figure I.1: Comparison of *BrIC* scores between researchers performing MBIM

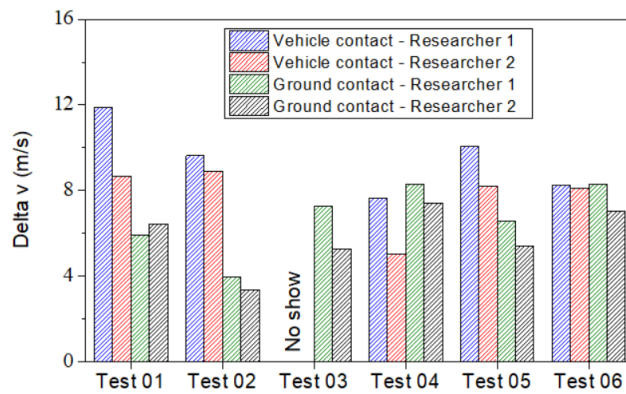


Figure I.2: Comparison of linear velocity changes between researchers performing MBIM

515

516

517

Table I.1-1: Intraclass correlation coefficients for two independent MBIM researchers for vehicle contact

	Test 01 Vehicle contact			Test 02 Vehicle contact			Test 03 Vehicle contact			Test 04 Vehicle contact			Test 05 Vehicle contact			Test 06 Vehicle contact		
	Pos	Lin Vel	Ang Vel	Pos	Lin Vel	Ang Vel	Pos	Lin Vel	Ang Vel	Pos	Lin Vel	Ang Vel	Pos	Lin Vel	Ang Vel	Pos	Lin Vel	Ang Vel
X	0.928	0.335	0.844	0.995	0.325	0.945	NA	NA	NA	0.993	0.965	0.005	0.998	0.969	-1.402	0.998	0.567	0.984
Y	-0.048	0.95	NA	0.948	0.774	0.888	NA	NA	NA	-0.107	-0.371	0.981	0.749	0.901	0.967	0.749	0.64	NA
Z	0.992	0.98	NA	0.978	0.762	-0.015	NA	NA	NA	0.959	0.99	0.091	0.988	0.987	0.963	0.988	0.954	NA

518

Table I.1-2: Intraclass correlation coefficients for two independent MBIM researchers for ground contact

	Test 01 Ground contact			Test 02 Ground contact			Test 03 Ground contact			Test 04 Ground contact			Test 05 Ground contact			Test 06 Ground contact		
	Pos	Lin Vel	Ang Vel	Pos	Lin Vel	Ang Vel	Pos	Lin Vel	Ang Vel	Pos	Lin Vel	Ang Vel	Pos	Lin Vel	Ang Vel	Pos	Lin Vel	Ang Vel
X	0.992	0.335	-0.124	0.998	0.325	0.36	0.975	0.937	-3.142	0.994	0.965	0.982	0.998	0.985	0.949	0.997	0.567	0.002
Y	0.977	0.95	0.05	0.969	0.774	0.691	0.877	0.582	0.906	0.582	-0.002	0.982	0.312	0.249	0.968	0.721	0.64	0.874
Z	0.995	0.98	0.919	0.938	0.762	0.933	0.996	0.649	0.841	0.964	0.99	0.929	0.971	0.99	-0.023	0.958	0.954	-0.061

519

520 **Appendix J: Estimated head ground contact stiffness.**

521 Table J1 shows the tests in which the ground contact mechanisms were suitable for estimating head
 522 ground contact stiffness. Consequently, Table J2 shows the reasons for the remaining tests.

523

Table J1: Contact location for suitable cadaver tests

Suitable Tests	Impact Location
Test 01	Occipital/parietal bone
Test 04	Chin
Test 05	Occipital/parietal bone

524

Table J2: Reasons for unsuitable cadaver tests

Unsuitable Tests	Reason
Test 02	Force goes through the head and head, preventing head rebound
Test 03	Facial padding adds damping
Test 06	Acceleration is not available

525

526 Table J.3 shows the head ground contact stiffness basing on the following equation and assuming a
 527 head mass (M) of 4.5kg:

528
$$k = \frac{M}{(\Delta t)^2} \left[\pi^2 + (1ne)^2 \right] ,$$

529 where e is the coefficient of restitution, which is defined as the rebound velocity divided by the
 530 velocity prior to contact. Values of pre/post impact velocity were taken from the MBIM results.

531

532

533

534

Table J.3: Head ground contact stiffness

Suitable Tests	Velocity before (m/s)	Velocity after (m/s)	e	Δt (ms)	k (kN/m)
Test 01	-5	0.75	0.15	5.9	1741
Test 04	-4	2.75	0.69	15.9	178
Test 05	-4.5	1.25	0.28	5.5	1709

535

536

537